Ellipsometric study of the optical properties of n-type superconductor $La_{1.9}Ce_{0.1}CuO_4$

Minglin Zhao,[1] Jie Lian,[1*] Zhaozong Sun,[1] Wenfu Zhang,[1] Mengmeng Li,[1] Ying Wang,[1] Heshan Yu,[2] Kui Jin,[2] and Xueyuan Hu[1]

[1]*Department of Optical Engineering, Shandong University, Jinan 250100, China*
[2]*National Lab for Superconductivity, Institute of Physics, Chinese Academy of Sciences, Beijing 100190, China*
[*] *opticsdu@163.com*

Abstract: Two thin $La_{2-x}Ce_xCuO_4$ (x = 0.1) films were deposited on [001]-oriented $SrTiO_3$ substrates by pulsed-laser deposition. The as-prepared LCCO films were well studied by X-ray diffraction, atomic force microscopy, transmission electron microscopy and spectroscopic ellipsometry. Spectroscopic ellipsometry provides a nondestructive, fast, and accurate method to explore the optical properties of the superconductive materials. The thickness and the optical dispersion model of the LCCO films in the visible range are presented for the first time. The results show that minor differences in the annealing progress will cause a relatively large change in the optical properties of the LCCO films.

OCIS codes: (160.4760) Optical properties; (310.6860) Thin films, optical properties.

References and links

1. Y. Tokura, H. Takagi, and S. Uchida, "A superconducting copper oxide compound with electrons as the charge carriers," Nature **337**(6205), 345–347 (1989).
2. R. A. Hughes, Y. Lu, T. Timusk, and J. S. Preston, "Normal-state optical properties of $Nd_{1.85}Ce_{0.15}CuO_{4+\delta}$," Phys. Rev. B Condens. Matter **47**(2), 985–990 (1993).
3. A. Pimenov, A. V. Pronin, A. Loidl, A. Tsukada, and M. Naito, "Peak in the far-infrared conductivity of strongly anisotropic cuprates," Phys. Rev. B **66**(21), 212508 (2002).
4. R. Henn, C. Bernhard, A. Wittlin, M. Cardona, and S. Uchida, "Far infrared ellipsometry using synchrotron radiation: the out-of-plane response of $La_{2-x}Sr_xCuO_4$," Thin Solid Films **313**, 642–648 (1998).
5. R. Henn, J. Kircher, M. Cardona, A. Wittlin, V. H. M. Duijn, and A. A. Menovsky, "Far-infrared c-axis response of $La_{1.87}Sr_{0.13}CuO_4$ determined by ellipsometry," Phys. Rev. B Condens. Matter **53**(14), 9353–9358 (1996).
6. A. Pimenov, A. V. Pronin, A. Loidl, A. Tsukada, and M. Naito, "Far-infrared and submillimeter-wave conductivity in electron-doped cuprate $La_{2-x}Ce_xCuO_4$," arXiv preprint cond-mat/0212400, 2002.
7. M. I. Alonso, M. Garriga, S. Piñol, and M. Brinkmann, "Doping dependence of the ellipsometric spectra of $Nd_{2-x}Ce_xCuO_{4-\delta}$ single crystals," Physica C **299**(1-2), 41–51 (1998).
8. M. I. Alonso, S. Tortosa, M. Garriga, and S. Piñol, "Ellipsometric measurement of the dielectric tensor of $Nd_{2-x}Ce_xCuO_{4-\delta}$," Phys. Rev. B **55**(5), 3216–3221 (1997).
9. T. Arima, Y. Tokura, and S. Uchida, "Optical spectra of $Pr_{2-x}Ce_xCuO_{4-\delta}$ crystals: Evolution of in-gap states with electron doping," Phys. Rev. B Condens. Matter **48**(9), 6597–6603 (1993).
10. E. M. Motoyama, G. Yu, I. M. Vishik, O. P. Vajk, P. K. Mang, and M. Greven, "Spin correlations in the electron-doped high-transition-temperature superconductor $Nd_{2-x}Ce_xCuO_{4\pm\delta}$," Nature **445**(7124), 186–189 (2007).
11. P. K. Mang, S. Larochelle, A. Mehta, O. P. Vajk, A. S. Erickson, L. Lu, W. J. L. Buyers, A. F. Marshall, K. Prokes, and M. Greven, "Phase decomposition and chemical inhomogeneity in $Nd_{2-x}Ce_xCuO_{4\pm\delta}$," Phys. Rev. B **70**(9), 094507 (2004).
12. S. Kuroshima, M. Fujita, T. Uefuji, M. Matsuda, and K. Yamada, "Phase diagram of the electron-doped superconductor $Pr_{1-x}LaCe_xCuO_{4-\delta}$," Physica C **392**, 216–220 (2003).
13. S. D. Wilson, S. Li, P. Dai, W. Bao, J. H. Chung, H. J. Kang, S. H. Lee, S. Komiya, Y. Ando, and Q. Si, "Evolution of low-energy spin dynamics in the electron-doped high-transition-temperature superconductor $Pr_{0.88}LaCe_{0.12}CuO_{4-\delta}$," Phys. Rev. B **74**(14), 144514 (2006).
14. K. Oka, H. Shibata, S. Kashiwaya, and H. Eisaki, "Crystal growth of $La_{2-x}Ce_xCuO_4$," Physica C **388**, 389–390 (2003).
15. M. Fujita, M. Nakagawa, C. D. Frost, and K. Yamada, "High-energy spin excitations in heavily electron-doped $Pr_{1-x}LaCe_xCuO_4$," J. Phys. Conf. Ser. **108**, 012006 (2008).

#244232 Received 2 Jul 2015; revised 25 Aug 2015; accepted 25 Aug 2015; published 31 Aug 2015

16. A. N. Lavrov, H. J. Kang, Y. Kurita, T. Suzuki, S. Komiya, J. W. Lynn, S. H. Lee, P. Dai, and Y. Ando, "Spin-flop transition and the anisotropic magnetoresistance of $Pr_{1.3-x}La_{0.7}Ce_xCuO_4$: unexpectedly strong spin-charge coupling in the electron-doped cuprates," Phys. Rev. Lett. **92**(22), 227003 (2004).
17. J. Yuan, H. Wang, I. Iguchi, Y. Hsu, S. Arisawa, A. Ishii, and T. Hatano, "Growth of electron-doped superconductor films and their applications to intrinsic josephson junctions," Applied Superconductivity, IEEE Trans. Appl. Supercond. **19**, 3443–3446 (2009).
18. F. J. Xia, Y. J. Fu, J. Yuan, H. Wu, Z. Xie, B. Xu, L. X. Cao, B. R. Zhao, and B. Y. Zhu, "Rectifying characteristic of perovskite oxide $La_{1.89}Ce_{0.11}CuO_4/Ba_{0.5}Sr_{0.5}TiO_3/La_{0.67}Sr_{0.33}MnO_3$ heterostructures," J. Appl. Phys. **110**, 103716 (2011).
19. H. Wu, L. Zhao, J. Yuan, L. X. Cao, J. P. Zhong, J. Gao, B. Xu, P. C. Dai, B. Y. Zhu, X. G. Qiu, and B. R. Zhao, "Transport properties of electron-doped $La_{2-x}Ce_xCuO_4$ cuprate thin films," Phys. Rev. B **73**(10), 104512 (2006).
20. A. Sawa, M. Kawasaki, H. Takagi, and Y. Tokura, "Electron-doped superconductor $La_{2-x}Ce_xCuO_4$: Preparation of thin films and modified doping range for superconductivity," Phys. Rev. B **66**(1), 014531 (2002).
21. M. Rahlenbeck, M. Wagenknecht, A. Tsukada, D. Koelle, R. Kleiner, B. Keimer, and C. Ulrich, "Raman light scattering study and microstructural analysis of epitaxial films of the electron-doped superconductor $La_{2-x}Ce_xCuO_4$," Eur. Phys. J. B **75**(4), 461–467 (2010).
22. J. S. Kim and D. R. Gaskell, "The phase stability diagrams for the systems $Nd_2CuO_{4-\delta}$ and $Nd_{1.85}Ce_{0.15}CuO_{4-\delta}$," Physica C **209**(4), 381–388 (1993).
23. S. Logothetidis, "Surface-roughness and grain-boundary effects on the optical properties of low-pressure chemical-vapor-deposited silicon thin films by spectroscopic ellipsometry," J. Appl. Phys. **65**(6), 2416–2426 (1989).
24. D. van der Marel, "Anisotropy of the optical conductivity of high-T_c cuprates," Phys. Rev. B **60**(2), 765–768 (1999).
25. Z. Sun, J. Lian, S. Gao, W. Xiao, Y. Wang, and X. Yu, "Complex refractive index and thickness characterization based on ant colony algorithm and comprehensive evaluation function," J. Comput. Theor. Nanosci. **11**(3), 816–820 (2014).
26. H. J. Kang, P. Dai, B. J. Campbell, P. J. Chupas, S. Rosenkranz, P. L. Lee, Q. Huang, S. Li, S. Komiya, and Y. Ando, "Microscopic annealing process and its impact on superconductivity in T′-structure electron-doped copper oxides," Nat. Mater. **6**(3), 224–229 (2007).
27. M. K. Kelly, P. Barboux, J. Tarascon, and D. E. Aspnes, "Optical properties of copper-oxygen planes in superconducting oxides and related materials," Phys. Rev. B Condens. Matter **40**(10), 6797–6805 (1989).

1. Introduction

The n-typed high-T_c superconducting cuprates, with the formula $L_{2-X}Ce_xCuO_4$ (L = La, Pr, Nd, etc), have been extensively investigated since their discovery in 1989 [1]. Optical studies of properties of these cuprate-based high-T_c superconductors are mostly focused on optical conductivity in the far-infrared [2–5] and submillimeter-wave regions [6] where optical response changes dramatically upon entering the superconducting state. Optical responses of these materials in the visible and near-uv energy regions, which could provide information about the transitions between electronic states, are relatively less available. Furthermore, most experimental studies in this region have been performed in $Nd_{2-X}Ce_xCuO_4$ crystals [7, 8] and $Pr_{2-X}Ce_xCuO_4$ crystals [9], because it is relatively easy to fabricate a high-quality single crystal of NCCO [10, 11] and PLCCO [12, 13] at present. There are few reports about the optical constants of LCCO in the visible region. The pure T'-phase single crystal of LCCO is still not available as far as we know [14–16]. Generally, the LCCO epitaxial thin films in the T'-phase with excellent quality can be prepared as an alternative.

In the present paper, LCCO thin films were prepared by pulsed laser deposition (PLD) on $SrTiO_3$ substrates. We report on ellipsometric measurements of the LCCO films in the visible region and present a Cauchy model combined with three Lorentz oscillators to describe the dispersion model of the LCCO films. The thicknesses of the LCCO films were independently analyzed by spectroscopic ellipsometry (SE) and transmission electron microscopy (TEM). X-ray diffraction (XRD) and atomic force microscopy (AFM) were performed to characterize the microstructure and the surface morphology of the samples. The presented optical constants show that the differences of the annealing process could result in changes in the morphology and optical properties.

2. Experimental method

The c-axis oriented films of electron-doped cuprates were deposited directly on the [001]-oriented $SrTiO_3$ substrate by a pulsed laser deposition system and we optimized the annealing

#244232 Received 2 Jul 2015; revised 25 Aug 2015; accepted 25 Aug 2015; published 31 Aug 2015

process to achieve high transition temperature. Some details of the preparation of the thin films can be found elsewhere [17, 18]. We studied two high quality samples annealed in high vacuum between 10^{-5} and 10^{-6} Torr. The thickness of the films is about 100nm and the detailed parameters are listed in Table 1. The zero-resistance superconducting transition temperature was measured by a Physical Property Measurement System (PPMS). For sample A, the T_c is 22K, and for sample B the T_c is 24K.

Table 1. The detailed parameters for samples.

	component	Desired thickness	annealing time	Tc
Sample A	0.1	100nm	180s	22K
Sample B	0.1	100nm	150s	24K

The phase and crystallinity of the LCCO thin films was characterized by X-ray diffraction (D8 Advance, Bruker AXS) with Cu-Kα = 1.54184 Å radiation. The surface topography was measured by atomic force microscopy (NaioAFM, Nanosurf, Switzerland). The LCCO thin films were studied by a rotating analyzer ellipsometer (GES5, SOPRA) with a XYZ moving stage and focusing probes (with the microspot size of 360*470um) at room temperature. The ellipsometric data were acquired in the wavelength range of λ = 300-800nm with a spectral resolution of 10nm at an angle of incidence $\theta = 75.07^{\circ}$. In the analyses, the commercial software WINWILL was used. The sum of a Cauchy model and a set of Lorentzian oscillators is used to describe our data. Furthermore, a point to point fitting at each individual wavelength based on ant algorithm was employed to analyze the ellipsometric data. A high resolution transmission electron microscope (HRTEM, Hitachi, H-9000NA) was employed to confirm the thickness of the films.

3. Results and discussion

3.1. XRD analyses of the LCCO

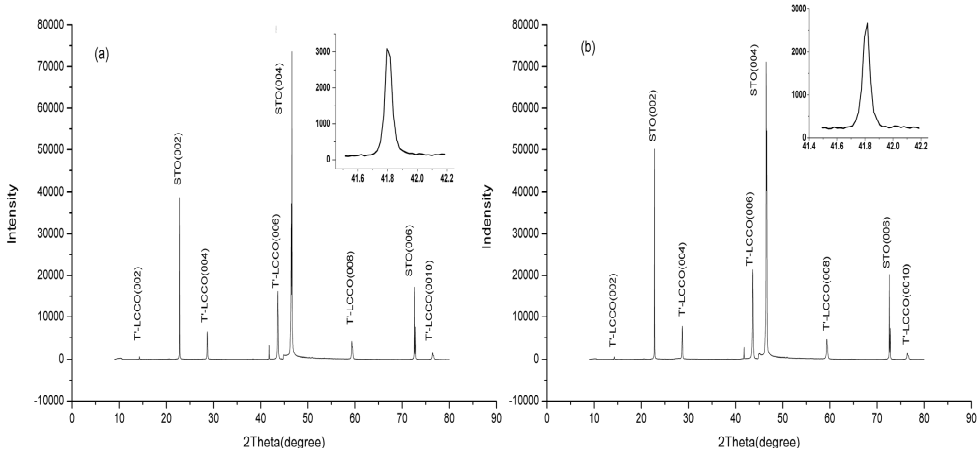

Fig. 1. XRD spectra of the LCCO thin films grown on (001) STO substrate, (a) Sample A (b) Sample B; the inset shows the rocking curve of the (006) peaks.

Figure 1 exhibits the XRD $\theta - 2\theta$ pattern of the two LCCO thin films deposited on (001) STO substrate. From the XRD data, we have not found any peak feature of T-phase of LCCO and the LCCO has T'-phase structure. The superconductivity in LCCO samples is present in T'-phase, which can be obtained by proper annealing treatments to remove the apical oxygen ions in a CuO_6 octahedron of T-phase. The locations of the corresponding peaks of the two samples are exactly identical, which indicates the same doping amount of the two samples. The full width at half maximum of the (006) XRD peaks are about 0.101 degree

#244232 Received 2 Jul 2015; revised 25 Aug 2015; accepted 25 Aug 2015; published 31 Aug 2015

and 0.125 degree, respectively, which reveals that both LCCO films exhibit good c-axis orientation.

3.2 Surface morphology analyses of the LCCO

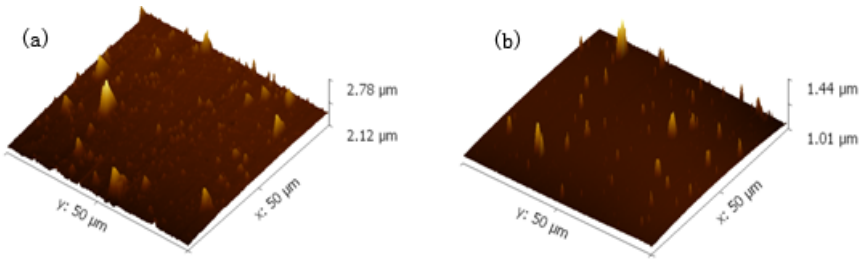

Fig. 2. AFM images of the LCCO films. (a) Sample A (b) Sample B.

Figure 2 shows the surface morphology of the samples characterized by atomic force microscopy. We clearly find many particle-like precipitates on the surface, which have already been discovered by others [19–21]. The particles have proven to be centers of Cu content, i.e. CuO_x (Cu_2O or CuO) [21]. As suggested by Kim and Gaskell [22], LCCO is unstable toward decomposition and produces Cu_2O during the annealing process. Interestingly, they also found that superconductivity only appeared in case that CuO is converted to Cu_2O in the binary system Cu-O. There are more particles on sample A than on sample B, and this phenomenon results from the different annealing process of these two samples. The particles, which bestrew the surface of the films, could be treated as the surface roughness, and the differences in surface roughness could lead to small changes in the amplitudes of the optical constants [23].

3.3 SE analyses of the LCCO

In any ellipsometry experiment, the Fresnel reflection coefficient ratio ρ is measured, and the two quantities tan ψ and cosΔ are related to the change of polarization state upon reflection, or the Fresnel reflection coefficient ratio ρ :

$$\rho = \chi_i \Big/ \chi_r = \tan\psi \cdot \exp(i\Delta) \tag{1}$$

where χ_i and χ_r correspond to the incident and reflected light polarization states, respectively. In the general case of reflection ellipsometry, the matrix describing the process is non-diagonal, where the elements include the mixture of s and p polarizations upon reflection, as can be seen by:

$$\begin{bmatrix} E_p^r \\ E_s^r \end{bmatrix} = \begin{bmatrix} r_{pp} & r_{ps} \\ r_{sp} & r_{ss} \end{bmatrix} \begin{bmatrix} E_p^i \\ E_s^i \end{bmatrix} \tag{2}$$

However, for special anisotropic orientations such as a uniaxial material with its optic axis parallel to the sample normal, no mixing between s and p polarization can occur so that $r_{sp} = r_{ps} = 0$, and materials behave as isotropic so that the equivalent optical constants can be obtained in this case. For oxygen deficient LCCO (and all other high-T_c cuprates), the crystal structure is uniaxial and optical anisotropy exists in the dielectric tensor components representing the c-axis and a-b plane direction [3, 24]. For expitaxial thin films, it is rather impossible to independently obtain the c-axis component and ab-axis component by ellipsometric measurement. Fortunately, in the present case, our samples are oriented with the optical axis perpendicular to the surface so that we can treat the samples as isotropic films to obtain the equivalent optical constants. The equivalent optical constants contain all the

#244232 Received 2 Jul 2015; revised 25 Aug 2015; accepted 25 Aug 2015; published 31 Aug 2015

spectral features of a-b planes and the influence of the c-axis is small [7]. For the ambient-LCCO-STO system, with the known STO dielectric function obtained by ellipsometric measurement before film deposition, the equivalent optical constants are easy to achieve.

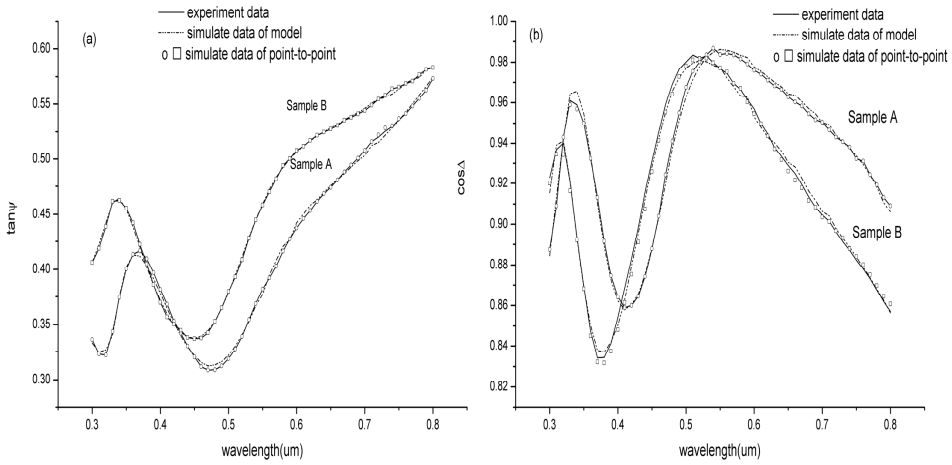

Fig. 3. Experimental tanψand cosΔ curves with best-fit theoretical curves (a) curves for tanψ(b) curves for cosΔ.

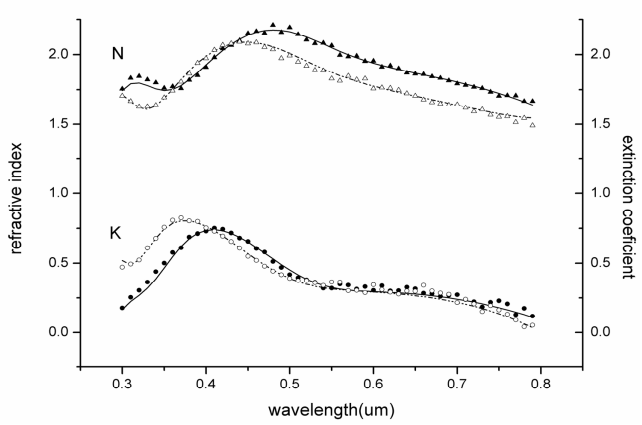

Fig. 4. The equivalent optical functions n and k shown for both an optical dispersion model and a point-by-point fit. Solid line (Sample A); Dash line (Sample B); Scatter (point-by-point).

Equation (1) and Eq. (2), which describe the relationship among optical parameters, thickness and the outputs of measurement (tan ψ and cos Δ, shown in Fig. 3) are nonlinear transcendental equations. The inversion method to analyze the ellipsometric data is commonly performed by fitting a model to describe the dependence of the refraction index (n) and coefficient extinction (k) on wavelength and tuning the parameters and film thickness until the simulated ellipsometric data match the experimental data. Nevertheless, this requires a deep understanding of physical and optical properties of the materials to build a proper dispersion model. For unknown materials such as the LCCO films, firstly, a point-to-point fitting, which could directly analyze the data at each individual wavelength without building a dispersion model, was performed over the range 300-800nm, keeping the thickness around 100nm. The discrete points in Fig. 4 show the results of point-to-point fitting and the values of n and k provide an initial exploration to the trend of the dispersion curve. In this paper, the point-to-point regression is based on a novel algorithm, the ant colony algorithm (ACA). This algorithm is used to solve the inversion problem by stimulating the food-seeking behavior by

#244232 Received 2 Jul 2015; revised 25 Aug 2015; accepted 25 Aug 2015; published 31 Aug 2015

ants. It has great advantages, such as parallelism, positive feedback, strong global optimum capacity and easily integrated with other algorithms. More details of the algorithm had been published elsewhere [25]. Then, through employing the point-to-point fitting result as a reference, Cauchy dispersion and three Lorentz oscillators are built. The Cauchy models are given by the expressions:

$$n(\lambda) = A + B/\lambda^2 + C/\lambda^4 \tag{3}$$

$$k(\lambda) = D + E/\lambda^2 + F/\lambda^4 \tag{4}$$

The Lorentz oscillators are given by the expressions:

$$\xi_r = A * \lambda^2 * \left(\lambda^2 - L_0^2\right) \Big/ \left[\left(\lambda^2 - L_0^2\right)^2 + \gamma^2\lambda^2\right] \tag{5}$$

$$\xi_i = A * \lambda^3 * \gamma \Big/ \left[\left(\lambda^2 - L_0^2\right)^2 + \gamma^2\lambda^2\right] \tag{6}$$

where A corresponds to the amplitude, L_0 to the central wavelength (um) and γ to the width of the peak, respectively. In Fig. 4, the results of the model are shown as smooth curves and the results have a great consistency with that of the point-to-point regression, furthermore, ensuring the Kramers-Kronig consistency of the calculated optical constants and reducing the noise effects. The best fitting parameters to use in the Cauchy and Lorentz models are shown in Table 2 and Table 3 below.

Table 2. The best fitting parameters in the Cauchy model for samples.

	A	B	C	D	E	F
Sample A	3.304395	0.1334	–0.021151	0.216979	0.104842	–0.006287
Sample B	3.30652	0.114038	–0.014654	0.339915	0.055428	–0.0021492

Table 3. The best fitting parameters in the Lorentz oscillators for samples.

		A	L_0	γ
Sample A	Peak 1	–4.879113	0.322794	0.169434
	Peak 2	–0.889145	0.517222	0.238436
	Peak 3	4.874852	1.340954	–0.379312
Sample B	Peak 1	–5.287993	0.299775	0.150580
	Peak 2	–1.330905	0.492413	0.274191
	Peak 3	2.522810	1.113794	–0.53172

Figure 4 reveals that at about 0.42um n decreases while k becomes enhanced and a broadened peak at about 410nm of Sample A and about 380nm of Sample B can be observed in the curves of the extinction coefficient. For superconducting oxides with copper-oxygen planes, the changes in the optical constants below 3eV are clearly dominated by the free carriers, and the peak features at higher energies are associated with the interband transitions involving electronic states in the CuO_2 planes [26]. However, the band structure is complicated, and the origin of the sharp features around 3eV is unclear. The two samples have the same doping concentration which can be confirmed by XRD, and the influence of thickness effect for the optical constants is small. For electron-doped copper oxide superconductors, the process of annealing slightly repairs Cu deficiencies in the as-grown materials and creates oxygen vacancies in the stoichiometric CuO_2 planes [27]. The annealing process could shift the effective electron-doping level and significantly increase electron mobility [27]. All of the above might affect the optical constants. For the foregoing reasons, the obvious shift of the broad peak at around 3eV can be mainly ascribed to the annealing process, but there is still confusion about how does it affect the optical constants. Further

#244232 Received 2 Jul 2015; revised 25 Aug 2015; accepted 25 Aug 2015; published 31 Aug 2015

studies on the interpretation of the relationship between annealing process and the band structure will be done in the future.

3.4 TEM analyses of the LCCO

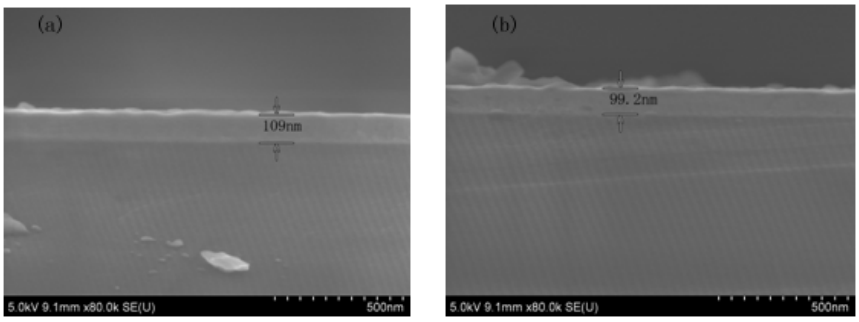

Fig. 5. Cross-sectional TEM images of the LCCO films. (a) Sample A (b) Sample B.

Compared to the AFM images, the surface roughness and impurity island could also be revealed by the TEM images in Fig. 5(b). The TEM thickness measurements, shown in Fig. 5, indicate that the thickness of the samples is 109nm and 99.2nm, respectively. The fitting results of the model indicate that the thickness of the samples is 109.7nm and 101.2nm, respectively. A relatively good agreement between the values from SE and the TEM is observed, confirming that the SE thickness is accurate. It must be pointed out that the TEM observations were not made in the same area with the SE measurement. In the inversion process of the ellipsomtric data, the surface roughness and the surface oxide layer is ignored. The difference between the two methods is mostly related to these factors.

4. Conclusion

In summary, spectroscopic ellipsometry allows the determination of the optical properties and thickness of LCCO thin films from wavelength of 300nm to 800nm at room temperature. Compared with the TEM and SE measurements, TEM sample preparation is difficult and time-consuming, but SE is a very fast, noninvasive, contactless, accurate and information-rich technique. Among the various characterization tools at the nanoscale, spectroscopic ellipsometry offers much more than measuring thickness, the determination of the complex refractive index gives access to a variety of sample properties, including fundamental physical parameters, chemical composition, and electrical conductivity. By applying an experimental approach, we have obtained the equivalent optical constants which can be well described with the sum of a Cauchy model and three Lorentzian oscillators. The differences in the process of annealing lead to the shift of the peak in higher energy range 2~4eV, which includes the changes in Cu-O planes of LCCO thin films.

Acknowledgments

This work is supported by grants from National Key Basic Research Program of China, No.2015CB921003 and fundamental research funds of Shandong University under grants No.2014TB018

#244232 Received 2 Jul 2015; revised 25 Aug 2015; accepted 25 Aug 2015; published 31 Aug 2015